Thermal Properties of Bi Nanowire Arrays with Different Orientations and Diameters

Yonggang Zhu, Xincun Dou, Xiaohu Huang, Liang Li, and Guanghai Li*

Key Laboratory of Materials Physics, Anhui Key Laboratory of Nanomaterials and Nanostructure Institute of Solid State Physics, Chinese Academy of Sciences, Hefei 230031, P. R. China

Received: August 14, 2006; In Final Form: September 29, 2006

The thermal properties of single-crystalline Bi nanowire arrays with different orientations and diameters were studied by differential scanning calorimeter and in situ high-temperature X-ray diffraction. Bi nanowires were fabricated by a pulsed electrodeposition technique within the porous anodic alumina membrane. The relationships between the orientation and diameter of Bi nanowires and the corresponding thermal properties are deduced solely from experimental results. It is shown that the melting point decreases with decreasing nanowire diameter, and there is an anisotropic thermal expansion property of Bi nanowires with different orientations and diameters. The transition of the thermal expansion coefficient from positive at low temperature to negative at high temperature for Bi nanowire arrays was analyzed and discussed.

Introduction

Nanowires are very interesting building blocks for nanoscale devices.[1] Devices and components such as field effect transistors, decoders, inverters, UV sensors, LEDs, lasers, chemical sensors, and biosensors[2−10] based on nanowires have been demonstrated. The nanowires could be used as components to create electrical circuits that are capable of being formed into extremely small circuits.[11] The exact knowledge of thermal properties of nanowires will be very important for application in nanowire devices.

The semimetal Bi is often selected for the study of fundamental quantum transport phenomena due to the very small electron density, highly anisotropic Fermi surface, small effective carrier masses, and long carrier mean-free path.[12,13] The electronic, magnetic, and thermoelectric properties of Bi nanowires have been extensively studied,[14−17] but the thermal properties of Bi nanowires are still widely unexplored. The physical properties of Bi nanowires strongly depend on not only the diameter but also the orientation of nanowires as well. Previous experimental studies focused mainly on the effect of diameter, and no report was found on the orientation of Bi nanowires. In our previous report the lattice parameter and thermal expansion coefficient of [110]-oriented Bi nanowires with a diameter ranging from 10 to 250 nm have been reported.[18] In this paper, as an extension of our previous study, we report the thermal properties of Bi nanowire arrays with different orientations and diameters.

Experimental Section

The anodic alumina membrane (AAM) was prepared using a two-step anodization process as described previously.[19−23] After the second anodization, the AAM was etched by saturated $SnCl_4$ solution to remove the remaining aluminum. The alumina barrier layer was then dissolved in a 5 wt % H_3PO_4 solution at 36 °C for 40 min. The AAMs with pore sizes of about 12, 36, and 60 nm were prepared. Finally, a layer of Au film (about 200 nm in thickness) was sputtered on one side of the AAM to serve as the cathode in a two-electrode plating cell, and a graphite plate was used as the counter electrode.

TABLE 1: Deposition Parameters of Bi Nanowire Arrays with Different Orientations

voltage (V)	pulsed time (ms)	duty (%)	orientation
−1.5	80	75	[104]
−1.9	50	75	[110]
−1.1	40	25	[202]

The electrolyte for the deposition of Bi nanowires contains a mixture of $BiCl_3$ (40 g/L), tartaric acid (50 g/L), glycerol (100 g/L), NaCl (70 g/L), and HCl (1 mol/L). The pH of the electrolyte was adjusted to about 0.9 by adding appropriate amounts of aqueous ammonia (5 mol/L) in order to avoid corrosive attack on the AAM. The pulsed electrodeposition was carried out under modulated voltage control, and detailed preparation conditions of Bi nanowires with different orientations can be found in Table 1.

The growth orientation of Bi nanowires was characterized using a X-ray diffractometer (Philips X'Pert) with Cu $K\alpha_1$ radiation. The morphologies of the Bi nanowire arrays were observed with field-emission scanning electron microscopy (FE-SEM, JEOL JSM-6700F). For X-ray diffraction (XRD) measurements the overfilled nanowires on the surface of the AAM template were mechanically polished away. The melting point of Bi nanowire arrays was measured by differential scanning calorimeter (Pyris Diamond DSC). In situ high-temperature XRD measurement was performed in the temperature range from 300 to 500 K under a high-vacuum atmosphere for the Bi nanowires inside the AAM. Temperatures were kept constant at each point for 20 min before measurement, and scans were carried out for $20° < 2\theta < 80°$. For SEM observations, the AAM was partly dissolved with 5 wt % NaOH solution and then carefully rinsed with deionized water several times.

Results and Discussion

The XRD patterns of Bi nanowires with different orientations and diameters are shown in Figure 1. It can be seen that all diffraction peaks can be indexed to the rhombohedral Bi (JCPDS No. 85-1331). The sharp and narrow XRD peaks indicate that

* To whom correspondence should be addressed. Fax: +86-551-5591434. E-mail: ghli@issp.ac.cn.

10.1021/jp0652493 CCC: $33.50
Published on Web 11/30/2006

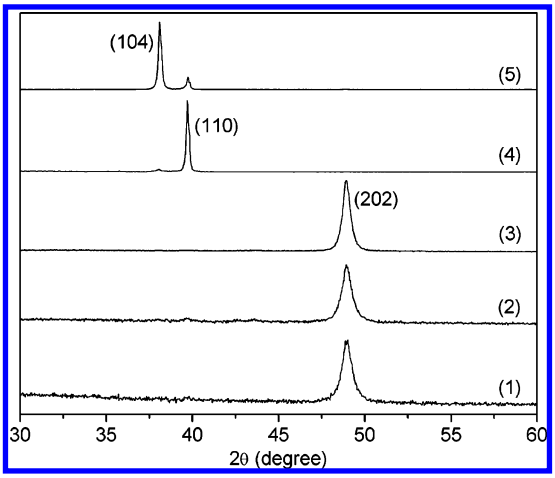

Figure 1. XRD patterns of Bi nanowire arrays with different orientations and diameters: (1) 12, (2) 36, and (3−5) 60 nm.

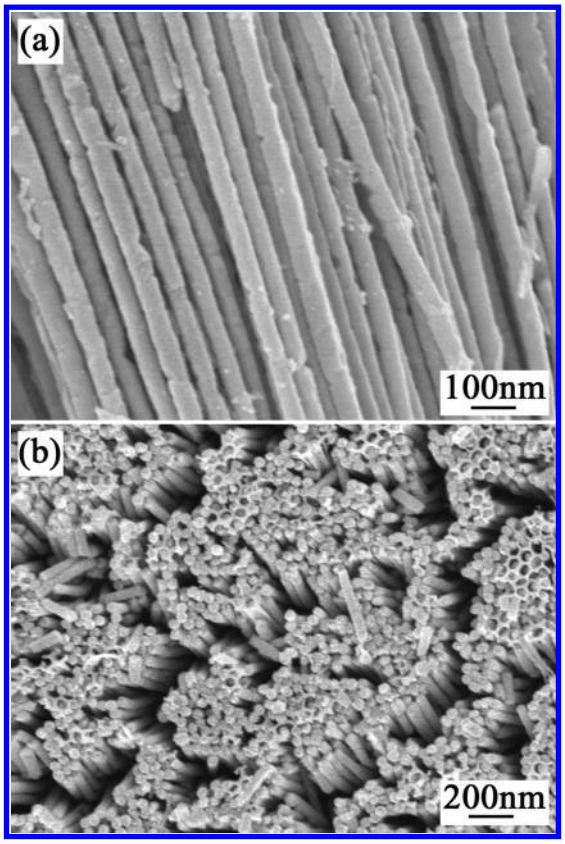

Figure 2. FESEM photographs of Bi nanowire arrays with different diameters: (a) 36 and (b) 60 nm.

the nanowires have good crystalline order, and the peaks at about $2\theta = 38.1°$, 39.7°, and 48.9° are very strong as compared with other peaks, indicating a highly preferential orientation of the nanowires, respectively, along the [104], [110], and [202] direction. No position shift of the XRD diffraction peak was found for Bi nanowires with the same orientation but different diameters. Clearly, the five Bi nanowire arrays can be divided into two groups, one with the same orientation but different diameters (curves 1−3 in Figure 1) and another with the same diameter but different orientations (curves 3−5 in Figure 1).

The FE-SEM images of Bi nanowires are shown in Figure 2. One can see that high filling, ordered, and uniform Bi nanowires were produced in the AAMs. Complete filling of Bi nanowires into the pores of AAM can be clearly observed in Figure 2b after AAM was partly dissolved.

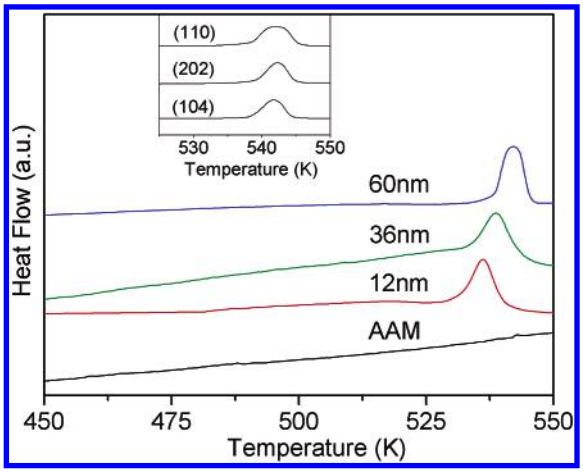

Figure 3. DSC traces of Bi nanowire arrays with different diameters together with those that form empty AAM. (inset) Those with the same diameter but different orientations. The curves were shifted in the *Y* axis direction for clarity.

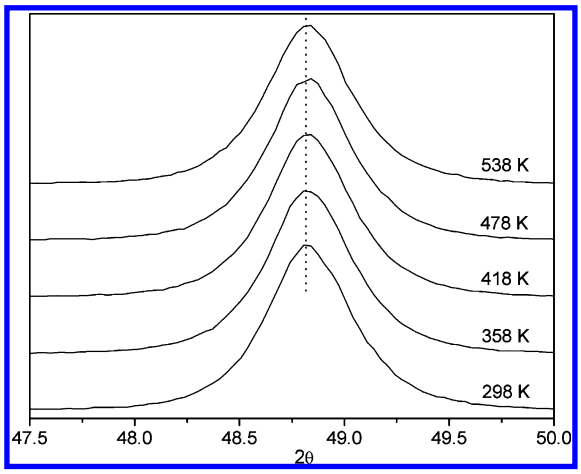

Figure 4. High-temperature XRD patterns of Bi nanowire arrays with a diameter of 12 nm at different temperatures.

Figure 3 shows heating measurement DSC curves of Bi nanowire arrays with different diameters. There is one endothermic peak located about the melting point of Bi that appears in each curve, and the peak is related to the melting fusion of Bi nanowires. The melting points of Bi nanowires with 12, 36, and 60 nm in diameter are found to be 536, 539, and 542 K, respectively, which all are lower than that of bulk Bi (544 K). The fact that the melting point of Bi nanowires with the same diameter but different orientation nearly has the same value, see the inset in Figure 3, indicates that the melting point of Bi nanowires is size dependent and independent of the orientation and shifts to low temperature with decreasing diameter. The difference in the heat of fusion with different diameters is considered the main reason for the size-dependent melting point.[24] The size-dependent melting point also has been observed in Zn nanowire arrays.[25] Being embedded inside the AAM, the thermal stress caused by the different thermal expansion coefficient between the nanowires and AAM will affect the melting point of the nanowires; however, these factors do not affect the comparison of the relative melting points of the nanowires with different diameters.

Figure 4 shows XRD patterns of the Bi nanowire array with a diameter of 12 nm at different temperatures, which shows that though there are delicate changes in the peak shape, the Bi nanowires preserve a rhombohedral lattice structure as compared with the standard diffraction of bulk bismuth, and no structure

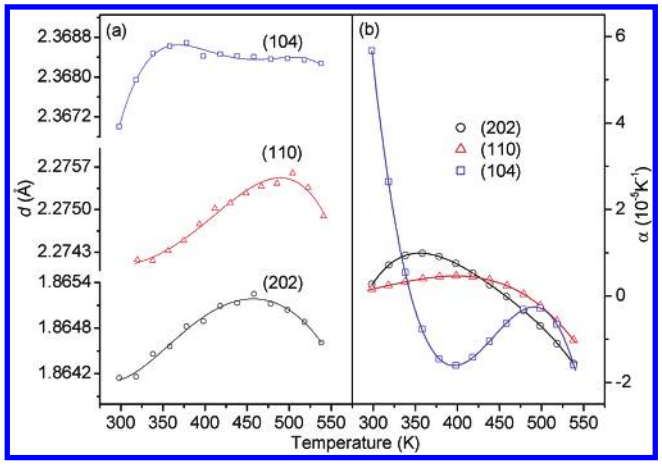

Figure 5. Temperature dependences of lattice parameter (a) and thermal expansion coefficient (b) of Bi nanowires with the same diameter but different orientations.

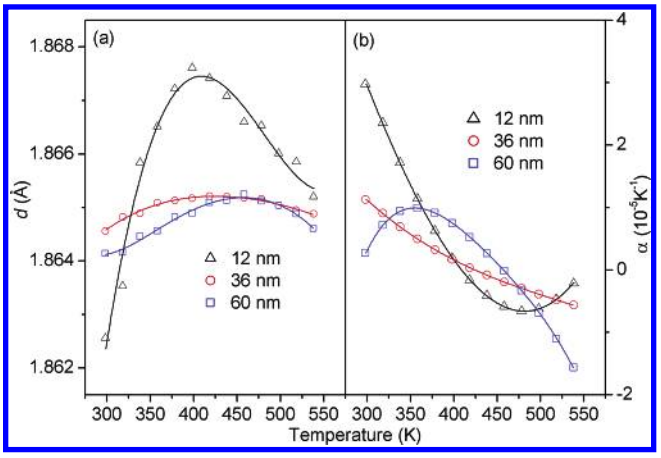

Figure 6. Temperature dependences of lattice parameter (a) and thermal expansion coefficient (b) of Bi nanowires with the same orientation but different diameters.

change has happened in the entire measuring temperature range. It is worth noting that the sample temperature is generally lower than the measured temperature due to the sample setup in the XRD measurement. Nevertheless, this factor does not affect the change trend of the measured lattice parameter with temperature. The existence of the XRD trace at 538 K might indicate this temperature difference, though the temperature is higher than the melting point obtained by DSC measurement.

The lattice parameter, d, can be calculated from the XRD pattern and Bragg equation, $2d \sin \theta = \lambda$. The exact position of the XRD peak of Bi nanowires at each temperature has been calibrated against the XRD peak taken on Pt. After fitting the experimental data with the fourth-order polynomial, $d = \sum_{n=0}^{4} a_n T^n$, the obtained coefficients, a_n, can be used to calculate the thermal expansion coefficient. The thermal expansion coefficient is defined by[26]

$$\alpha = \frac{1}{d_0}\frac{\partial d}{\partial T} = \frac{1}{d_0}(a_1 + 2a_2T + 3a_3T^2 + 4a_4T^3) \qquad (1)$$

Figure 5 shows temperature dependences of lattice parameter and thermal expansion coefficient of Bi nanowire arrays with the same diameter (60 nm) but different orientations. One can see that the lattice parameter nonlinearly depends on temperature and increases with temperature at low temperature after reaching a maximum value and then decreases at high temperature. The thermal expansion coefficient also nonlinearly depends on temperature, and there is a transition from a positive thermal expansion coefficient at low temperature to a negative one at high temperature. The transition temperature is about 345, 459, and 491 K for Bi nanowires with an orientation of [104], [202], and [110], respectively. An anisotropic thermal expansion behavior of Bi nanowires with different orientations was demonstrated for the first time in the present study.

The temperature dependences of lattice parameter and thermal expansion coefficient of Bi nanowires with the same orientation ([202]) but different diameters are shown in Figure 6. For [202]-orientated Bi nanowires, the transition temperature of the thermal expansion coefficient from positive to negative is about 409, 425, and 459 K with a diameter of 12, 36, and 60 nm, respectively. The result shows that the transition temperature shifts to high temperature with increasing diameter of Bi nanowires, which has the same feature as reported in our previous study.[18]

To study the influence of defects and stresses on the thermal properties, we measured the lattice parameter of 60 nm Bi nanowires with [202] orientation the second time after the first time measurement, and the result is shown in Figure 7. It is worth noting that the maximum measuring temperature (538 K) is lower than the melting point of the nanowires (542 K), and thus, no melting happened after the first time measurement. From Figure 7 one can clearly see three features: (1) the lattice parameter of the Bi nanowires at the second time is lower than that at the first time in the whole temperature range studied, (2) the temperature dependence of the lattice parameter measured at the second time becomes weak as compared with that at the first time, (3) the lattice parameters in the second time measurement at temperature higher than 500 K are even lower than that at room temperature. The lattice parameters of all Bi nanowires at room temperature before and after high-temperature measurements are summarized in Table 2. From this table one can see that the room-temperature lattice parameter measured the second time is always smaller than at the first time for all nanowires studied. This result indicates that the defects, such as vacancies, impurities, and surface defects, might affect the thermal properties of the nanowires.

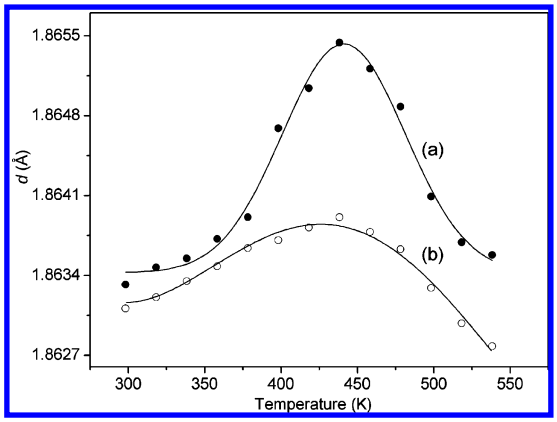

Figure 7. Temperature dependences of lattice parameter of Bi nanowires with a diameter of 60 nm measured at the first (a) and second time (b).

TABLE 2: Lattice Parameter of Bi Nanowires at Room Temperature Before and After High-Temperature XRD Measurements

sample	12 nm (202)	36 nm (202)	60 nm (202)	60 nm (110)	60 nm (104)
bulk	1.8624			2.2665	2.3579
before	1.8626	1.8639	1.8646	2.2742	2.3670
after	1.8606	1.8624	1.8645	2.2736	2.3667

There are always certain defects and lattice stresses in Bi nanowires, and with decreasing diameter the surface defects and tension will increase substantially. Defect and stress might be significant in determining the thermal behavior of nanowires. They are 'frozen' around room temperature. Timmesfeld and co-workers[27] studied the influence of vacancies on the thermal expansion of the solid state and found that the change of crystalline volume caused by vacancies is

$$\Delta V = BV_0 \exp[-Q/kT] \quad (2)$$

where Q, B, V_0, k, and T are, respectively, the formed energy of vacancies, constant, crystalline volume at 0 K, Boltzmann constant, and temperature, which shows that the lattice parameter will shrink with increasing temperature or upon annealing. Actually our first time XRD measurement is equivalent to an anneal process, which will partly eliminate the vacancies in Bi nanowires, and thus the lattice parameter will decrease at the second time measurement.

As is well known, most materials usually show a positive thermal expansion property with increasing temperature. This behavior can be understood by considering the effects of the anharmonic potential on the equilibrium lattice separations and is usually characterized by the Grueneisen parameter (for bulk Bi the Grueneisen parameter is always positive, so a positive thermal expansion coefficient is obtained).[28] The negative thermal expansion, which represents lattice contraction with temperature, was also observed among anisotropic systems,[29,30] where contraction along one crystallographic direction was usually accompanied by expansion along the others.[31]

Anisotropic properties of the thermal expansion of Bi nanowires can be understood by properties of binding forces between atoms. Different crystal directions have different packing densities, which is a significant factor in affecting the thermal expansion coefficient. The smaller the packing density, the larger the thermal expansion coefficient.[32] With increasing temperature, the thermal activation motion of atoms in Bi nanowires will increase and the electronic cloud of the crystal lattice will expand.[33] If the packing density is large, i.e., the space that is not filled by atoms in the crystal cell is small, the probability of inflated electronic clouds overlapping with each other will be large, the repulsion forces between atoms will be large, and thus the thermal expansion coefficient will be large. In contrast, if the packing density is small, the probability of inflated electronic clouds overlapping with each other will be small and thus the thermal expansion coefficient will be small. The packing density of the [202] direction of Bi nanowires is the highest and thus has the lowest thermal expansion coefficient, while [104] Bi nanowires have the highest thermal expansion coefficient in the room-temperature region.

In our previous study[18] the transition of the thermal expansion coefficient from positive at low temperature to negative at high temperature for Bi nanowire arrays was attributed to the effects of electronic excitations on the equilibrium lattice separation. In nanowires, the energy level spacing of the spatially confined valence electrons depends on the temperature. Lattice shrinking results in an increase in the level separation when the temperature is increased, which, on one hand, reduces the number of electrons occupying the excited states as dictated by the Fermi–Dirac factor and, on the other hand, raises the thermal energy of individual electrons in the excited states. These two factors compete delicately to achieve a lower electronic potential energy that results in the crossover from thermal expansion to thermal contraction.

The thermal expansion or thermal contraction upon heating depends on the balance between phonon modes with positive and negative Grueneisen parameters. Transverse acoustic (TA) modes might exhibit negative Grueneisen parameters related to the increase of the restoring forces with increased tension.[34] Because TA modes represent the lowest frequency modes, thermal contraction is more often seen only well below the Debye temperature. In the present study the transition of the thermal expansion coefficient from positive to negative is well above the Debye temperature of bulk Bi (119 K). Nevertheless, in nanometer scale, for Bi nanowires some unusual low-energy phonons might be activated at temperatures well above the Debye temperature and contribute to the thermal contraction,[35] and these unusual low-energy phonons might be diameter dependent. The smaller the diameter, the lower the temperature of the appearance of the unusual low-energy phonons. Study of the vibration modes of Bi nanowires at different temperatures is needed to understand the thermal contraction of Bi nanowires with increasing temperature.

Being embedded inside the pores of the AAM, the nanowires would experience biaxial compressive stresses in the inward radial direction and induced tensile uniaxial stresses in the growth direction due to both the restriction of the AAM wall and the thermal stress by the different thermal expansion coefficient between the nanowires and AAM, which will affect the thermal expansion behavior of Bi nanowires and lead to an increase in the thermal expansion coefficient. Nevertheless, the thermal stress at the direction normal to the nanowire axis is much higher than that along the nanowire, and restriction of the AAM wall will mainly affect transverse expansion of the nanowires, while in our study we measure the longitudinal expansion and thus the influence of the restriction of the AAM wall, and the thermal stress on the thermal expansion of the Bi nanowires is much less.

Conclusions

We successfully prepared Bi nanowire arrays with different orientations and diameters by pulsed electrodeposition in the pores of AAM. It was found that the melting point of Bi nanowires decreases with decreasing nanowire diameter. Our results clearly show an anisotropic thermal expansion property of 60 nm Bi nanowires with different orientations, and there is a transition from a positive thermal expansion coefficient at low temperature to a negative one at high temperature for Bi nanowire arrays with different orientations and diameters. Our results proved for the first time from experimental data that the physical properties of Bi nanowires depend strongly on the orientation of the nanowires.

Acknowledgment. This work was supported by the National Natural Science Foundation of China (no. 10474098) and the National Major Project of Fundamental Research for Nanomaterials and Nanostructures (no.: 2005CB623603).

References and Notes

(1) Xia, Y. N.; Yong, P. D.; Sun, Y. G.; Wu, Y. Y.; Mayers, B.; Gates, B.; Yin, Y. D.; Kim, F.; Yan, H. Q. *Adv. Mater.* **2003**, *15*, 353.

(2) Goldberger, J.; Hochbaum, A. I.; Fan, R.; Yong, P. *Nano Lett.* **2006**, *6*, 973.

(3) Zhong, Z. H.; Wang, D. L.; Cui, Y.; Marc, W.; Bockrath; Lieber, C. M. *Science* **2003**, *02*, 1377.

(4) Cui, Y.; Lieber, C. M. *Science* **2001**, *291*, 851.

(5) Suehiro, J.; Nakagawa, N.; Hidaka, S.; Ueda, M.; Imasaka, K.; Higashihata, M.; Okada, T.; Hara, M. *Nanotechnology* **2006**, *17*, 2567.

(6) Duan, X.; Huang, Y.; Cui, Y.; Wang, J.; Lieber, C. M. *Nature* **2001**, *409*, 66.

(7) Pauzauskie, P. J.; Sirbuly, D. J.; Yang, P. D. *Phys. Rev. Lett.* **2006**, *96*, 143903.
(8) Greytak, A. B.; Barrelet, C. J.; Li, Y.; Lieber, C. M. *Appl. Phys. Lett.* **2005**, *87*, 151103.
(9) Liu, H.; Kameoka, J.; Czaplewski, D. A.; Craighead, H. G. *Nano Lett.* **2004**, *4*, 671.
(10) Byon, H. R.; Choi, H. C. *J. Am. Chem. Soc.* **2006**, *128*, 2188.
(11) Friedman, R. S.; McAlpine, M. C.; Ricketts, D. S.; Ham, D.; Lieber, C. M. *Nature* **2005**, *434*, 1085.
(12) Yang, F. Y.; Liu, K.; Hong, K.; Reich, D. H.; Searson, P. C.; Chien, C. L. *Science* **1999**, *284*, 1335.
(13) Hicks, L. D.; Harman, T. C.; Dresselhaus, M. S. *Appl. Phys. Lett.* **1993**, *63*, 3230.
(14) Zhang, Z.; Sun, X.; Dresselhaus, M. S.; Ying, J. Y. *Appl. Phys. Lett.* **1998**, *73*, 1589.
(15) Heremans, J.; Thrush, C. M.; Zhang, Z.; Sun, X.; Dresselhaus, M. S.; Ying, J. Y.; Morelli, D. T. *Phys. Rev. B* **1998**, *58*, 10091.
(16) Heremans, J.; Thrush, C. M. *Phys. Rev. B* **1999**, *59*, 12579.
(17) Lin, Y. M.; Sun, X. Z.; Dresselhaus, M. S. *Phys. Rev. B* **2000**, *62*, 4610.
(18) Li, L.; Zhang, Y.; Yang, Y. W.; Huang, X. H.; Li, G. H.; Zhang, L. D. *Appl. Phys. Lett.* **2005**, *87*, 031912.
(19) Jin, C. G.; Zhang, G. Q.; Qian, T.; Li, X. G.; Yao, Z. *J. Phys. Chem. B* **2004**, *108*, 1844.
(20) Zhang, Y.; Li, G. H.; Wu, Y. C.; Zhang, B.; Song, W. H.; Zhang, L. D. *Adv. Mater.* **2002**, *14*, 1227.
(21) Li, L.; Yang, Y. W.; Huang, X. H.; Li, G. H.; Zhang, L. D. *J. Phys. Chem. B* **2005**, *109*,12394.
(22) Li, L.; Li, G. H.; Zhang, Y.; Yang, Y. W.; Zhang, L. D. *J. Phys. Chem. B* **2004**, *108*, 19380.
(23) Liang, Y. Q.; Zhai, L.; Zhao, X. S.; Xu, D. S. *J. Phys. Chem. B* **2005**, *109*, 7120.
(24) Lai, S. L.; Guo, J. Y.; Petrova, V.; Ramanatch, G.; Allen, L. H. *Phys. Rev. Lett.* **1996**, *77*, 99.
(25) Wang, X. W.; Fei, G. T.; Zheng, K.; Jin, Z.; Zhang, L. D. *Appl. Phys. Lett.* **2006**, *88*, 173114.
(26) Saotome, T.; Ohashi, K.; Sato, T.; Maeta, H.; Haruma, K.; Ono, F. *J. Phys.: Condens. Matter* **1998**, *10*, 1267.
(27) Timmesfeld, K. H.; Elliott, R. J. *Phys. Stat. Sol. (B)* **1970**, *42*, 859.
(28) Ashcroft, N. W.; Mermin, N. D.; *Solid State Physics*; Saunders: Philadelphia, 1976.
(29) Mary, T. A.; Evans, J. S. O.; Vogt, T.; Sleight, A. W. *Science* **1996**, *272*, 90.
(30) Yamfamura, Y.; Nakajima, N.; Tsuji, T. *Phys. Rev. B* **2001**, *64*, 184109.
(31) Bailey, C.; Yates, B. *J. Appl. Phys.* **1970**, *41*, 5088.
(32) White, G. K.; Collocott, S. J.; Cook, J. S. *Phys. Rev. B* **1984**, *29*, 4778.
(33) Weinberg, S. *The Quantum Theory of Fields*; Cambridge University Press: New York, 1995.
(34) Barron, T. H. K. *Ann. Phys.* **1957**, *1*, 77.
(35) Hancock, J. N.; Turpen, C.; Schlesinger, Z.; Kowach, G. R.; Ramirez, A. P. *Phys. Rev. Lett.* **2004**, *93*, 225501.